




Cavity-enhanced absorption and dispersion spectroscopy of the 1238-nm line of H<sub>2</sub>H. Liang (梁慧),<sup>1</sup> Y. Tan (谈艳) ,<sup>2,\*</sup> C.-L. Hu (胡常乐),<sup>2</sup> Z.-L. Nie (聂中梁),<sup>2</sup> A.-W. Liu (刘安雯) ,<sup>1,3</sup>  
Y. R. Sun (孙羽),<sup>4</sup> J. Wang (王进),<sup>2</sup> and S.-M. Hu (胡水明) ,<sup>1,2,†</sup><sup>1</sup>Hefei National Laboratory, *University of Science and Technology of China, Hefei 230088, China*<sup>2</sup>Hefei National Research Center of Physical Sciences at the Microscale, *University of Science and Technology of China, Hefei 230026, China*<sup>3</sup>State Key Laboratory of Molecular Reaction Dynamics, Department of Chemical Physics,  
*University of Science and Technology of China, Hefei 230026, China*<sup>4</sup>*Institute of Advanced Science Facilities, Shenzhen 518107, China*

(Received 17 July 2024; accepted 19 September 2024; published 15 October 2024)

Doppler-broadened absorption and dispersion spectra of the Q(1) line in the first overtone band of H<sub>2</sub> were recorded together with a comb-locked cavity-enhanced spectroscopy instrument. On the basis of the Hartmann-Tran profile, the absorption and dispersion spectra were fitted independently, resulting in two consistent sets of line profile parameters. The intensities obtained by the two methods reached an accuracy below 0.1%, and agree well with the theoretical results. This work not only provides a test of high-level quantum chemistry calculations of the simplest neutral molecule, but also demonstrates the potential for SI-traceable high-precision molecular density measurements based on laser spectroscopy.

DOI: [10.1103/PhysRevA.110.042817](https://doi.org/10.1103/PhysRevA.110.042817)

## I. INTRODUCTION

The hydrogen molecule, as the simplest and calculable neutral molecule, is a benchmark for testing quantum chemistry theories and calculations. By employing *ab initio* calculations along with quantum electrodynamics (QED) theory, one can accurately compute the transition frequencies and intensities of hydrogen molecules. These calculations act as standards for experimental validation [1–5]. In the last decade, molecular hydrogen transition frequencies have also been precisely measured [6–16], and related advances can be found in a recent review [17]. The experimental transition frequencies agree excellently with the theoretical calculations, and the discrepancies are at 10<sup>−9</sup>.

Precise line intensities and profiles of molecular hydrogen are also essential for various fields, including astronomical observations and the analysis of planetary atmospheres. Recent progress in SI-traceable spectroscopic methods has demonstrated line intensity measurements with a precision of 10<sup>−3</sup> [18], facilitating applications in gas metrology, such as determining molecular density (partial pressure) and temperature. The capability for *ab initio* calculations of molecular hydrogen with very high accuracy also holds significant promise for metrology. However, the very weak transition moments and the complicated line profiles of the hydrogen molecule hindered the accurate determination of the transition intensities. The rovibrational transitions of homonuclear hydrogen molecules (H<sub>2</sub> and D<sub>2</sub>) are extremely weak electric quadrupole transitions. Heteronuclear isotopologues have dipole transitions that are also weaker than conventional

transitions of other molecules in the same region by several orders of magnitude. The discrepancies between the existing experimental and calculated line intensities vary in the range of 1%–20% [19–24]. The significance of speed-dependent collision effects in the pressure-broadened spectra of molecular hydrogen is remarkable, making it an ideal candidate for evaluating collision-induced line-shape models. There have been several works on comparisons between *ab initio* calculations and experimental observations concerning collisional line-shape effects on H<sub>2</sub> lines broadened by rare gases [25–29].

In this study, we report spectroscopy measurements of a rovibrational absorption line of H<sub>2</sub> employing two distinct techniques but utilizing the same cavity-enhanced spectroscopy apparatus: absorption spectra via cavity ring-down spectroscopy (CRDS) and dispersion spectra through cavity mode dispersion spectroscopy (CMDS). Given that each method operates on different principles and has different characteristics, comparing their results enables the identification and correction of systematic errors. We chose the Q(1) line in the (2-0) band of H<sub>2</sub> around 1238 nm due to its relatively high line strength and good separation from other molecular transitions. Accurate measurement of the intensity of this line can be used to determine the density of hydrogen molecules with SI traceability. Additionally, the line profile parameters serve as important references for studies on precise line-shape theories.

## II. EXPERIMENTAL

The configuration of the experimental setup is shown in Fig. 1(a). The spectral laser source was a homemade external cavity diode laser (ECDL) tunable in the region of 1180–1280 nm. The optical cavity was about 52 cm long, corresponding to a free spectral range (FSR) of 290 MHz,

\*Contact author: [tanyan@ustc.edu.cn](mailto:tanyan@ustc.edu.cn)†Contact author: [smhu@ustc.edu.cn](mailto:smhu@ustc.edu.cn)

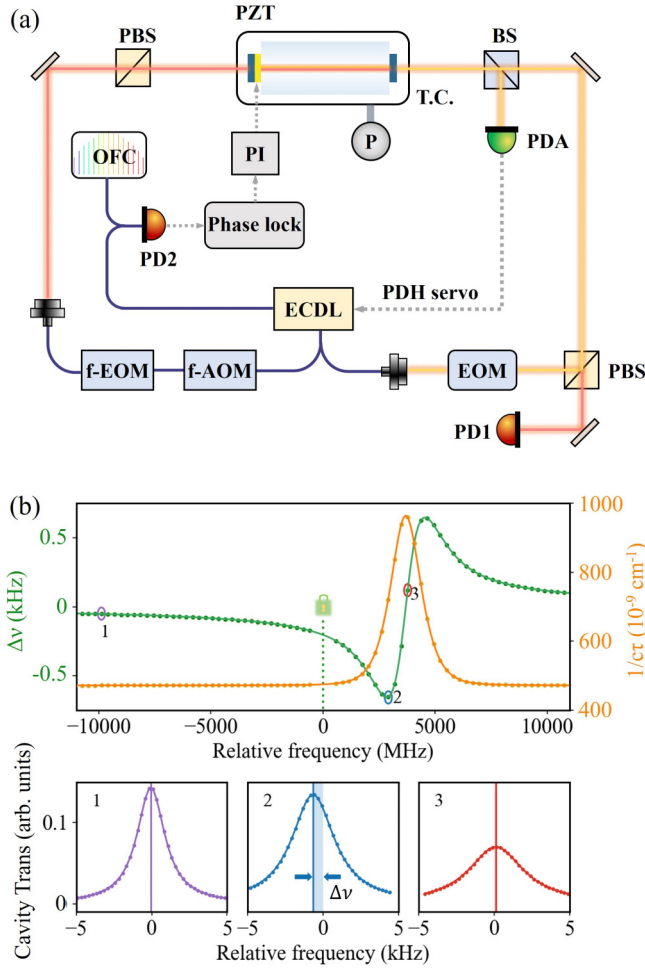


FIG. 1. (a) Configuration of the experimental setup for CRDS and CMDS measurements. BS: beam splitter; ECDL: external-cavity diode laser; EOM: electro-optic modulator; f-AOM: fiber acousto-optic modulator; OFC: optical frequency comb; P: pressure gauge; PBS: polarized beam splitter; PD: photodiode; PG: pressure gauge; PZT: piezoelectric actuator; TC: temperature control servo. (b) Schematic diagram of the absorption spectrum (orange) and dispersion spectrum (green). The transmittance spectra of three cavity modes labeled as 1–3 in the dispersion spectrum are given in the bottom panel.

and consisted of two concave mirrors with a reflectivity of 99.997%. The optical cavity was installed in an aluminum chamber temperature stabilized to about 298.36 K by a proportional-integral-derivative (PID) controller. The temperature was measured by two platinum thermosensors calibrated by the National Institute of Metrology (NIM, China). The temperature drift and the difference between both sensors were less than 5 mK, and the absolute uncertainty of temperature was 10 mK.

The ECDL laser output was divided into two beams with orthogonal polarizations. The *p*-polarized beam was phase modulated by an electro-optic modulator (EOM, Thorlabs EO-PM-NR-C2) with a modulation frequency of 23 MHz, and a Pound-Drever-Hall (PDH) [30] locking servo was applied to lock the laser to one cavity mode. The frequency of this mode is shown as “zero” in Fig. 1(b). This locking servo

can tightly lock the laser with the cavity, and as a result, the laser frequency also follows the drift of the cavity due to thermal expansions and vibrations. Therefore, we applied a second locking servo [“phase lock” block shown in Fig. 1(a)]. The beat frequency between the spectral laser and a tooth of the optical-frequency comb was recorded and referenced to a frequency source to generate the error signal. The feedback was applied to a piezoelectric actuator attached to one of the highly reflective mirrors to adjust the cavity length. The two servo loops eventually lock both the cavity and the laser frequency with the comb tooth. More details of such double-locking servos can be found in our previous work [31]. The *s*-polarized beam from the spectral laser was frequency shifted using a fiber acousto-optic modulator (f-AOM) and a fiber electro-optic modulator (f-EOM) and then coupled into the optical cavity for spectral analysis. The cavity transmission signal was detected by a photodiode detector (PD1). By varying the radio frequency  $f_{\text{EOM}}$  applied to the f-EOM and measuring the cavity’s transmittance, we can capture the transmission spectrum of the cavity around a specific mode. Several examples, including the transmission spectra of three cavity modes, are illustrated in the lower panels of Fig. 1(b), corresponding to different points indicated on the dispersion spectrum represented by the green curve in the upper panel. By fitting each spectrum with a Lorentzian function [32], we determined the mode frequency  $\nu_m = \nu_0 + f_{\text{AOM}} + f_{\text{EOM}}^m$ . Here,  $\nu_0$  is the frequency of the “zero” mode obtained from the beat note between the laser and the optical frequency comb, while  $f_{\text{AOM}}$  and  $f_{\text{EOM}}^m$  are the radio frequencies applied to the f-AOM and f-EOM, respectively.

For cavity modes that are far from molecular absorption lines, the transmission profile of the cavity can be modeled using the Airy formula [33,34]. The width of the cavity mode indicates the round-trip loss of the cavity [35]. Therefore, the gas absorption increases the loss and also the cavity mode width. Note that even at the center of the  $\text{H}_2$  absorption line, the width of the cavity mode is only a few kilohertz. Since the width of the  $\text{H}_2$  absorption line is about 1 GHz, the absorption coefficient could be considered constant within the range of a cavity mode, and the asymmetry in the mode profile due to molecular absorption is also negligible. As we only measure the exact center frequencies of the mode, we opted to fit the data using the Lorentzian function instead of the Airy function. The dispersion signal was obtained by comparing the change in the cavity mode frequency to that without absorption, as depicted in Fig. 1(b).

The ring-down spectrum was obtained by tuning one sideband generated by the f-EOM to match a cavity mode and switching off the f-AOM to initiate a ring-down event. The ring-down signal was captured using a digitizer (NI PXIe-5922), and the decay rate  $(c\tau)^{-1}$  was calculated by fitting the ring-down curve to a single exponential decay model. The absorption coefficient of the sample was determined by the difference in the decay rates. An example of a ring-down spectrum is shown as the orange curve in Fig. 1(b). The sensitivity of a CRDS instrument primarily depends on the cavity length  $L$  and the reflectivity  $R$  of the cavity mirrors, with the noise equivalent absorption coefficient  $\alpha_{\text{min}}$  proportional to  $\frac{1-R}{L}$ . In this work,  $\alpha_{\text{min}}$  was  $8 \times 10^{-12} \text{ cm}^{-1}$  with an averaging time of approximately 20 s.

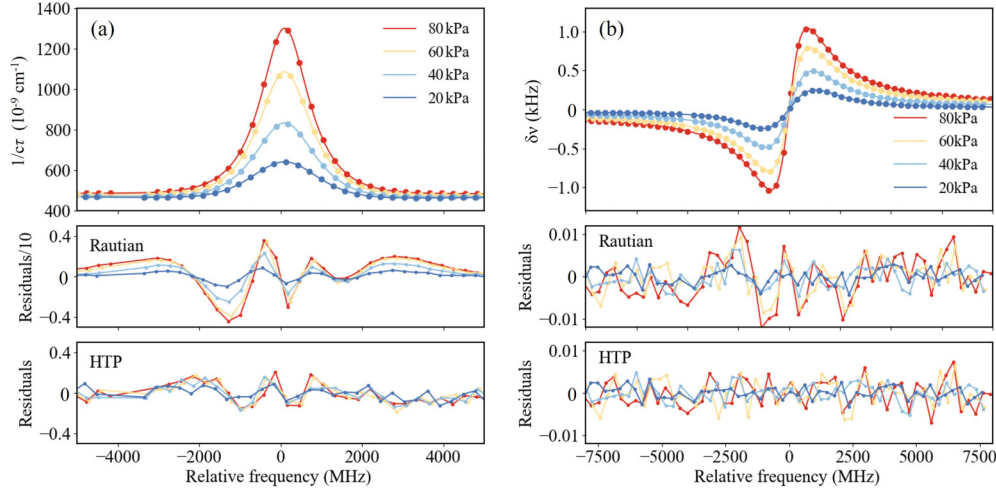


FIG. 2. (a) CRDS and (b) CMDS experimental spectra of the Q(1) (2-0) line of  $\text{H}_2$  at different pressures. The lower panels show the fitting residuals from the Rautian and HTP line-shape models, respectively.

A pure hydrogen gas sample (AirLiquid Co.) with a declared purity of 99.9999% was used and a liquid nitrogen trap was used to eliminate contaminants in the sample prior to use. The gas pressure of the sample was measured using a commercial capacitance manometer (Leybold CTR101N) for pressures below 1000 Torr. All rf sources in this study were synchronized with a GPS-disciplined rubidium clock with long-term stability of  $10^{-12}$ . The optical frequency comb was stabilized to a hydrogen maser with a fractional frequency drift of less than  $3 \times 10^{-16}$ /day.

### III. RESULTS AND DISCUSSION

We measured the Q(1) line in the first overtone band (2-0) of  $\text{H}_2$ . According to the HITRAN database, the transition frequency is  $8075.3074 \text{ cm}^{-1}$  and the line intensity is  $2.6 \times 10^{-27} \text{ cm/molecule}$ . Figure 2 shows the spectra recorded with sample pressures in the range of 10–80 kPa.

The absorption and dispersion spectra can be described as follows:

$$\alpha(\nu_m) = A \times \text{Re}[\varphi(\nu_m - \nu_c)] \quad (1)$$

$$\frac{\Delta\nu}{\nu_m} = \frac{A}{2nk_0} \times \text{Im}[\varphi(\nu_m - \nu_c)]. \quad (2)$$

The profiles of the absorption and dispersion spectra correspond to the real and imaginary components of the normalized line function  $\varphi(\nu_m - \nu_c)$  [34,36], respectively. Here,  $\nu_m$  represents the optical frequency of the  $m$ th cavity mode, which is the sum of the ECDL spectral laser frequency and the microwave frequency shift ( $f_{\text{AOM}} + f_{\text{EOM}}$ ). The ECDL laser frequency was determined by referencing the optical frequency comb.  $A$  denotes the area under the absorption line (amplitude),  $n$  is the refractive index that is independent of frequency,  $k_0$  is the wave vector associated with the transition frequency, and  $\Delta\nu$  is the frequency shift of the cavity mode caused by the dispersion effect of the molecular transition. The dispersion due to the cavity mirror can be considered

negligible [37] within approximately 10 GHz around the transition.

We analyzed the measured absorption and dispersion spectra using Eqs. (1) and (2), respectively, to determine the integral area  $A$  and the line profile parameters of the function  $\varphi(\nu_m - \nu_c)$ . Two line profiles, the Rautian profile [38,39] and the Hartmann-Tran profile (HTP) [40], were employed to fit the spectra. The Doppler widths were fixed to the theoretical values at the corresponding temperatures, while the line centers and other parameters were allowed to vary during the fitting. It is important to note that we ignored the correlation parameter of the speed-dependence effect and the velocity-changing (Dick-narrowing) effect, setting the parameter  $\eta$  to zero in the fitting process. Figure 2 presents the fitting results of the absorption and dispersion spectra. The findings indicate that the spectra of  $\text{H}_2$  are better fitted by the HTP line profile, which accounts for speed-dependent effects [41,42] and Dicke narrowing [43]. We used the fit quality factor [44]  $Q$  to assess the fit quality. For example, for the spectra recorded at 80 kPa, the  $Q$  factors for the HTP/Rautian profiles are 8889/640 for the absorption spectrum and 576/407 for the dispersion spectra, respectively. Despite the signal-to-noise ratio of the dispersion spectrum being 20 times lower than that of the absorption spectrum, we conclude that the HTP profile provides a better fit for the spectra compared to the Rautian profile.

We fitted each of the measured absorption and dispersion spectra at different pressures. Figure 3 presents the results for line parameters measured at various pressures: the pressure broadening half-width  $\Gamma_0$ , the pressure-induced shift  $\Delta_0$ , the line broadening  $\Gamma_2$ , the frequency shift  $\Delta_2$  due to velocity-dependent effects, and the velocity-changing collision parameter  $\nu_{\text{VC}}$ . Despite the independent fitting processes, the figure shows a strong agreement between the parameters derived from the absorption and dispersion spectra. All of the parameters of the line shape exhibit a strong linear dependence on the pressure within the bounds of the experimental uncertainties. The pressure widths  $\Gamma_0$  measured at various pressures demonstrate superior linearity compared to other

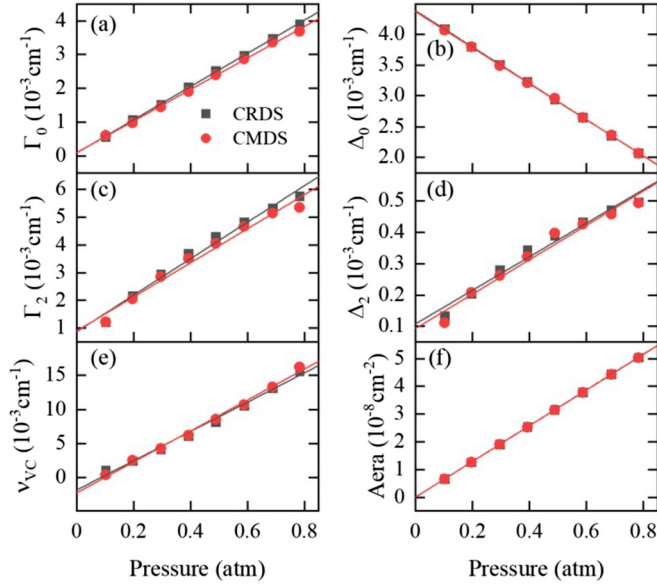


FIG. 3. Pressure dependence of the line parameters obtained by fitting the spectra of the Q(1) line at eight pressures: (a) self pressure-broadening width, (b) pressure-induced shift, (c) line broadening due to speed dependence, (d) line shift due to speed dependence, and (e) velocity-changing collisions parameter. The fitted spectrum areas are also linearly regressed in (f). Dark gray squares and red circles represent CRDS and CMDS data, respectively.

speed-dependent parameters, consistent with the findings of previous research [45–47].

The coefficients for the line shape are presented in Table I. The parameters derived from both the absorption and dispersion spectra generally show good agreement. It is important to note that the dispersion spectra are more sensitive to the profiles compared to the absorption spectra [48,49], indicating that the line parameters provided here are probably suitable. The pressure-induced shift coefficient  $\delta_0$  obtained in this study aligns well with the results of the HITRAN database [50], but shows significant differences from those reported by the Grenoble group [47]. It should be noted that the fitting methods in the two studies differ: the Grenoble group [47] employed a multispectra global fit, enforcing linear variation of parameters with pressure, while in this study, spectra mea-

TABLE I. Line-shape parameters obtained from fitting the CRDS and CMDS spectra with the HTP profile. The parameter  $\eta$  was set to be zero in the fit. The uncertainties given in parentheses correspond to the  $1\sigma$  statistical value from the linear fit. Unit:  $10^{-3} \text{ cm}^{-1} \text{ atm}^{-1}$ .

|            | This work |          | Grenoble <sup>a</sup> | HITRAN <sup>b</sup> |
|------------|-----------|----------|-----------------------|---------------------|
|            | CRDS      | CMDS     |                       |                     |
| $\delta_0$ | -2.944(8) | -2.92(2) | -3.25(2)              | -2.9(1)             |
| $\delta_2$ | 0.54(4)   | 0.55(4)  | 0.61                  | 1.2(1)              |
| $\nu_{VC}$ | 21.5(8)   | 22.7(7)  | 20.85                 | 48(2)               |
| $\gamma_0$ | 4.91(3)   | 4.66(7)  | 5.18                  | 4.3(2)              |
| $\gamma_2$ | 6.58(36)  | 6.15(37) | 7.18                  | 0.4                 |

<sup>a</sup>Results from Fleurbaey *et al.* [47]; uncertainties of  $\delta_2$ ,  $\nu_{VC}$ ,  $\gamma_0$ , and  $\gamma_2$  were not given there.

<sup>b</sup>Results from the HITRAN database [50].

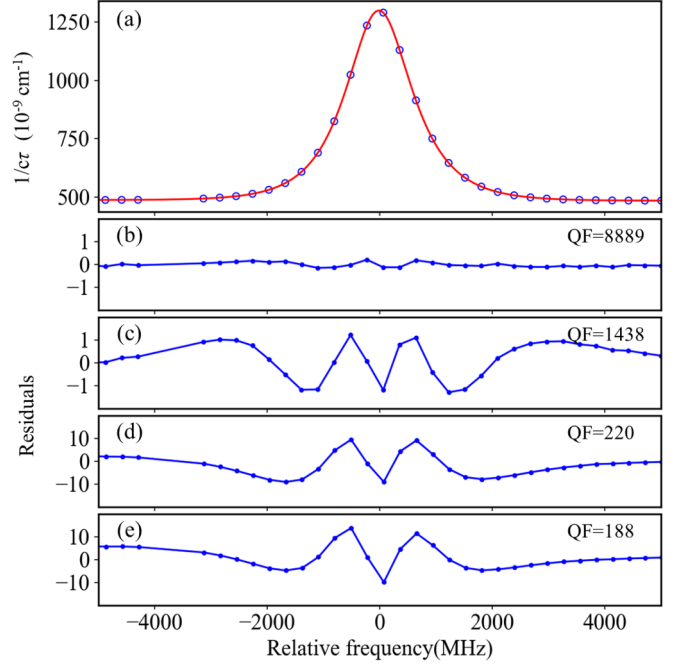


FIG. 4. (a) CRDS spectrum of the Q(1) (2-0) line of  $\text{H}_2$  at 80 kPa and (b)–(e) fitting residuals with different constraints of the line profile parameters: (b) relaxed the line-shape parameters except for the correlation parameter  $\eta$  set to be zero; (c) with boundary constraints for  $\gamma_2 \leq 2/3\gamma_0$  and  $\eta = 0$ ; (d)  $\nu_{VC}$  fixed to the HITRAN value and  $\eta = 0$ ; and (e)  $\nu_{VC}$  fixed to the HITRAN value,  $\eta$  relaxed, and the boundary constraint kept for  $\gamma_2 \leq 2/3\gamma_0$ .

sured at different pressures were fitted independently, and a linear fit of the parameters against pressure was used to obtain the coefficient, as illustrated in Fig. 3.

The pressure-induced line-broadening coefficient  $\gamma_0$  determined in this study is less than the value reported by the Grenoble group but greater than the HITRAN value. One possible reason for this discrepancy is that we relaxed all the line-shape parameters except for the correlation parameter  $\eta$ , which was set to zero during fitting. The pressure changes of  $\gamma_2$  and  $\nu_{VC}$  display complementary patterns, particularly at higher pressures. We hypothesize that the nonlinear dynamics of these two parameters, illustrated in Figs. 3(c)–3(e), probably arise from neglecting the correlation between speed-dependent effects and velocity-changing collisions. Correlations can distort the optimal fit parameters. Consequently, the speed-dependent line-broadening parameter  $\gamma_2$  exceeds the quadratic approximation, and the value of velocity-changing collisions  $\nu_{VC}$  is only half of the HITRAN value derived from the diffusion coefficient [46]. However, it is well known that for  $\text{H}_2$ , velocity-changing collisions are more significant than internal-state changes caused by inelastic collisions. We attempted to fit the spectra using the HTP profile under various conditions. We selected the CRDS spectrum at 80 kPa, which has the best signal-to-noise ratio. Initially, we fixed the correlation coefficient  $\eta$  to zero during fitting. Figure 4(b) shows the fitting residuals when all line-shape parameters were relaxed, resulting in a quality factor (QF) value of nearly 9000. When we imposed the constraint  $\gamma_2 \leq 2/3\gamma_0$ , the QF value dropped to less than 1500,

TABLE II. Position and intensity (pure H<sub>2</sub>, 296 K) of the Q(1) line in the (2-0) band of H<sub>2</sub>. The number given in parentheses in the unit of the last quoted digit corresponds to the (1 $\sigma$ ) uncertainty.

|                     | $\nu_c$<br>(kHz)      | $S_{296\text{K}} \times 10^{27}$<br>(cm/molecule) |
|---------------------|-----------------------|---|
| Calculated [5,50]   | 242 091 627 553(1499) | 2.600(3)  |
| Grenoble, CRDS [47] | 242 091 630 935(69)   | 2.6021(3) <sup>a</sup>                            |
| This work, CRDS     | 242 091 631 305(116)  | 2.6010(16)  |
| This work, CMDS     | 242 091 630 821(289)  | 2.5979(22)  |

<sup>a</sup>Only the statistical uncertainty; no systematic uncertainty was given in Ref. [47].

as shown in Fig. 4(c). Fixing  $\nu_{VC}$  to the HITRAN calculated value of 1091.93 MHz yielded a very low QF value of 220 [Fig. 4(d)]. We also tested with relaxing the  $\eta$  value while keeping  $\gamma_2 \leq 2/3\gamma_0$  and  $\nu_{VC} = 48 \times 10^{-3} \text{ cm}^{-1} \text{ atm}^{-1}$ , resulting in a QF value of only 188 and  $\eta \approx 1.00$ , with the fitting residuals shown in Fig. 4(e). In conclusion, a better fitting QF provides a more accurate determination of the integrated absorption area, but the line-shape parameters could be unphysical. Further investigation into the non-Voigt line-shape model is necessary, and our high-quality spectra recordings of pure hydrogen can serve as an ideal subject, since the collision effects for hydrogen can be calculated precisely with the *ab initio* methods.

To determine the line centers and amplitudes, we also individually fit the spectra measured at various pressures. By linearly extrapolating the line centers obtained at different pressures, we derived the transition frequency at the zero pressure limit, as shown in Table II. Note that our CRDS and CMDS line centers are in good agreement, but the uncertainty of the CMDS result is higher because of the lower signal-to-noise ratio in the spectra. Our CRDS result is approximately 0.4 MHz larger than the Grenoble result [47], but is still within three times the combined experimental uncertainties. The line centers obtained from Doppler-broadened spectroscopy in Grenoble [47] and in this work are slightly larger than the value of 242 091 630 140(9) kHz from Lamb-dip measurements [16,51] reported by the Amsterdam group. Our results are approximately 4 MHz larger than the *ab initio* calculated value [5], which is about 2.5 times the uncertainty of the calculation. This systematic deviation between experimental and theoretical results [17] indicates the need to consider high-order QED effects in the calculation.

The experimental peak area  $A$  obtained from fitting the spectra at a given temperature  $T$  and sample pressure  $P$  was used to determine the absorption line strength  $S(T)$  (in cm/molecule) according to  $A(T) = S(T)P/k_B T$ . Figure 5(a) shows the Allan deviations of the ratio between the intensity of the experimental line obtained at a sample pressure of 80 kPa and the calculated value [5,50]. We can see that the uncertainty of the results from the CMDS dispersion spectra (red) is significantly larger than that from the CRDS absorption spectra (dark gray). This is a result of a lower signal-to-noise ratio in the CMDS measurement. The statistical uncertainty of the averaged CMDS values continuously decreases to  $2 \times 10^{-4}$ , while the uncertainty of CRDS remains below  $1 \times 10^{-4}$ .

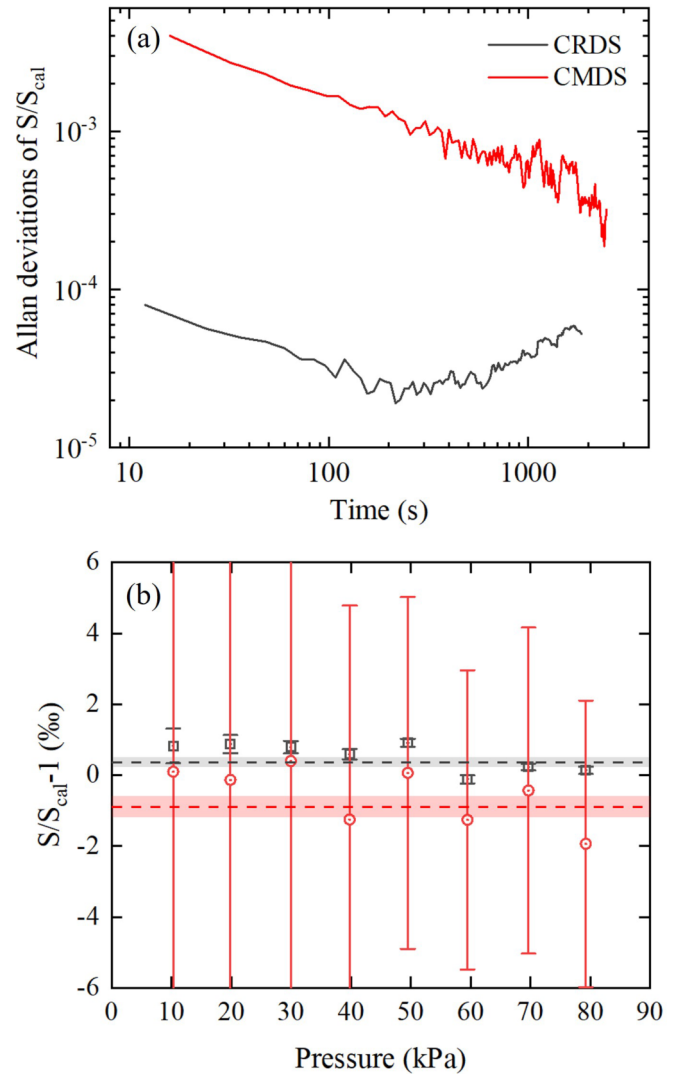


FIG. 5. (a) Allan deviations of the experimental line intensities obtained in this work. All experimental line-strength values were divided by the calculated value of  $2.600 \times 10^{-27} \text{ cm/molecule}$ . (b) The line intensities of Q(1) at 296 K obtained from fitting the absorption (CRDS) and dispersion (CMDS) spectra recorded at different pressures. The dashed lines correspond to the weighted average values, and the belts represent the statistical uncertainties  $1\sigma$ .

The line strength  $S(T)$  relates [50] to the transition rate—Einstein-A coefficient  $A_{21}$ ,

$$S(T) = \frac{g_2 \sigma_a c A_{21}}{8\pi \nu_0^2 Q_{\text{tot}}(T)} \frac{1}{e^{-\frac{E_1}{k_B T}} \left[1 - e^{-\frac{h\nu_0}{k_B T}}\right]}, \quad (3)$$

where  $k_B$  is the Boltzmann constant,  $h$  and  $c$  are the Planck constant and the speed of light,  $\nu_0$  is the transition frequency in hertz,  $E_1$  is the energy of the lower level of the transition,  $g_2$  is the statistical weight of the upper level,  $\sigma_a$  is the isotopic abundance, and  $Q_{\text{tot}}(T)$  is the partition sum [52,53] at temperature  $T$ . We converted  $S(T)$  to the strength  $S(T_0)$  at the HITRAN standard temperature of  $T_0 = 296 \text{ K}$  according to Eq. (3). The CRDS and CMDS results obtained at different pressures are shown in Fig. 5(b). It can be seen that the line intensities obtained by the two methods agree well with each other.

TABLE III. Uncertainty budget of line intensity of Q(1) at 296 K (unit: in  $10^{-3}$ ).

| Source             | $u_r$ (CRDS) | $u_r$ (CMDS) |
|--------------------|--------------|--------------|
|                    | Type A       |              |
| Statistical        | 0.1          | 0.3          |
|                    | Type B       |              |
| Temperature        | 0.05         | 0.05         |
| Pressure           | 0.12         | 0.12         |
| Line shape         | 0.2          | 0.6          |
| AOM temperature    | 0.5          | –            |
| Gas purity         | 0.01         | 0.01         |
| Isotopic abundance | 0.02         | 0.02         |
| Etalon effect      | 0.2          | 0.5          |
| <b>Total</b>       | <b>0.6</b>   | <b>0.85</b>  |

Table III gives the uncertainty budget of the line intensities for both the CRDS and the CMDS results. The statistical uncertainties (type A) are estimated to be  $1 \times 10^{-4}$  and  $3 \times 10^{-4}$  for CRDS and CMDS, respectively, according to the fitting uncertainties shown in Fig. 5(b). The main sources of systematic uncertainties (type B) are as follows.

(1) As shown in Fig. 6(a), the temperature drift during one measurement period is less than 5 mK, and the uncertainty in the calibration of the thermal sensor is below 10 mK, which contributes an uncertainty of  $5 \times 10^{-5}$  to the line intensity.

(2) The pressure gauge (Leybold) was calibrated by a reference manometer (Inficon, uncertainty  $3 \times 10^{-5}$ ) several times in the last year, and the deviations are shown in Fig. 6(b). The results indicate excellent stability of the calibrated gauge. We use the standard deviation  $1.2 \times 10^{-4}$  as the uncertainty in the pressure measurement.

(3) The uncertainty in the line-profile model also contributes to a systematic deviation in the line-intensity value. Here, we estimate the contribution according to the fitting varieties of the HTP profiles applied in the fitting. Under the signal-to-noise ratio level of about 8000:1 for CRDS and 1000:1 for CMDS, the uncertainties are  $2 \times 10^{-4}$  and  $6 \times 10^{-4}$  for the absorption and dispersion spectra, respectively.

(4) During the CRDS measurement, we discovered a correlation between the temperature of the f-AOM and the observed integrated absorbance. We speculate that the f-AOM has a small delay when it is turned off to trigger a ring-down measurement, and the delay shifts the observed ring-down time. The delay was measured to be less than 100 ns, but could be temperature dependent. We finally stabilized the temperature of the f-AOM in the measurement, but the systematic shift could still exist and we estimate an uncertainty of  $5 \times 10^{-4}$  in the CRDS result.

(5) The uncertainties due to gas purity and isotopic abundance are  $1 \times 10^{-5}$  and  $2 \times 10^{-5}$ .

(6) In cavity-enhanced spectroscopy measurements, the interferometric structure due to etalon effects [54], resulting in a sine-wave baseline in the observed spectra, can often be seen. We observed a very stable structure during measurements in almost half a year and attribute uncertainties of  $2 \times 10^{-4}$  and  $5 \times 10^{-4}$  to the line intensities obtained from the absorption

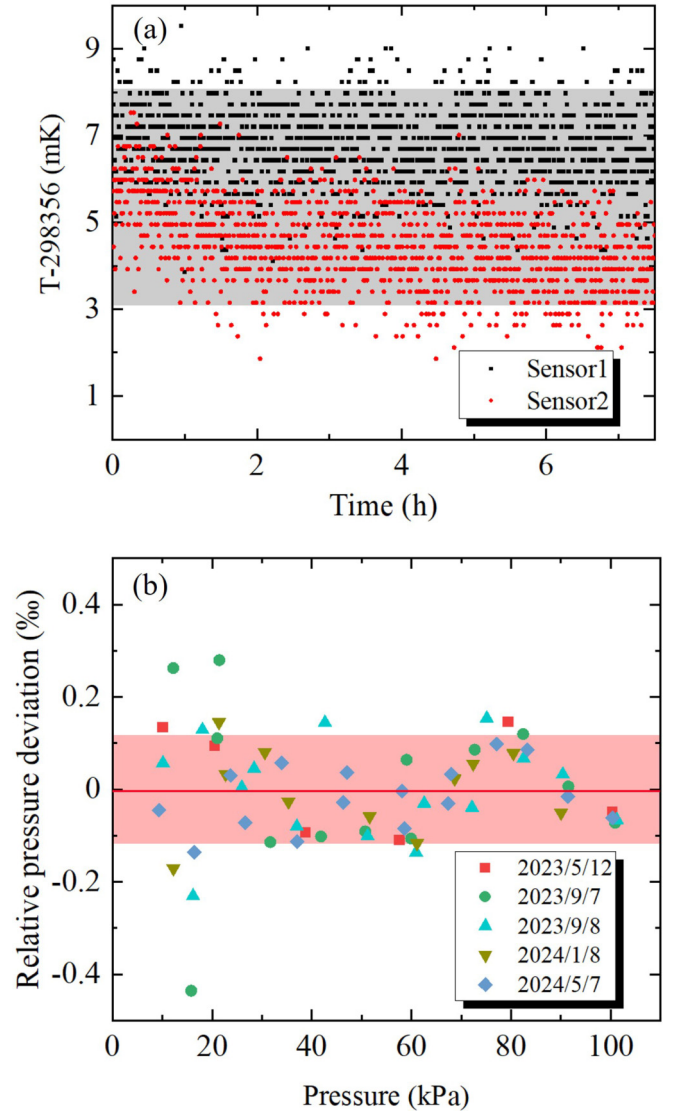


FIG. 6. (a) Cavity temperature drift measured by two PT100 thermal sensors. (b) Deviations between the readings of the calibrated Leybold gauge and the reference manometer. Different symbols indicate the calibration date.

and dispersion spectra, respectively. In total, the uncertainties are  $6 \times 10^{-4}$  and  $8.5 \times 10^{-4}$  for the intensities of the CRDS and CMDS lines, respectively. The line intensities of the Q(1) line in the (2-0) band of  $H_2$  obtained from CRDS and CMDS are given in Table II. Both results agree reasonably well with each other. The weighted average of the two values is

$$S_{Q(1),296K} = 2.5999(13) \times 10^{-27} \text{ cm/molecule.} \quad (4)$$

The result agrees well with the theoretical value [24] and the previous experimental result obtained by the Grenoble group [47].

The uncertainties in temperature and pressure measurements are currently at the level of  $1 \times 10^{-4}$ . In principle, these uncertainties could be reduced by an order of magnitude with more accurate calibrated gauges. The CRDS measurement has the potential to lower statistical uncertainty to  $10^{-5}$ . However, achieving this level of precision for systematic uncertainties is more challenging. To measure the decay time with sufficient

accuracy, a switcher with a rising time below 10 ns is essential. Additionally, an analog-to-digital converter with a wide dynamic range and excellent linearity is required. Moreover, reducing the amplitude of parasitic etalons in the optical path to  $1 \times 10^{-11} \text{ cm}^{-1}$  presents a significant challenge in optical design. In general, the all-frequency measurement character of CMDS offers substantial potential for improvement. Currently, the accuracy of CMDS measurements is primarily limited by the signal-to-noise ratio. The relatively high statistical uncertainty in CMDS also complicates the analysis of other systematic error sources, such as the line profile model and baseline distortion. Given that the amplitude of the dispersion spectrum is only a few kilohertz, achieving a precision of  $10^{-5}$  requires determining the cavity mode frequency with subhertz accuracy. Special measures must be taken to meet the requirement, including isolating the apparatus from mechanical vibrations and ambient noise. It is worth noting that CRDS and CMDS have very different sources of systematic errors. Therefore, cross-comparing measurements from both methods could be highly valuable for assessing uncertainties and evaluating results.

#### IV. CONCLUSION

In this work, we present the absorption and dispersion spectroscopy of the Q(1) transition of  $\text{H}_2$  around 1238 nm using a single cavity-enhanced spectroscopy setup. Precise

line intensities and line profile parameters were determined from both dispersion and absorption spectra, showing excellent agreement between the results from the two methods. The consistency of the results suggests that systematic errors in the experiment are well controlled. The reported experimental line intensity carries an uncertainty of less than 0.1%, which is primarily attributed to the limited control over experimental conditions and the line profile models used. Currently, the experimental results agree with the calculated values at the  $10^{-3}$  level, with the latter limited by the Born-Oppenheimer approximation adopted in the calculation [24]. Incorporating nonadiabatic and relativistic effects could improve the accuracy to the  $10^{-4}$  level, which can be addressed in future calculations. Progress in both experimental and theoretical methods will support advancements in primary gas metrology and provide a critical test of *ab initio* calculations for this four-body system.

#### ACKNOWLEDGMENTS

This work was jointly supported by the National Natural Science Foundation of China (Grants No. 12393825, No. 12393822, No. 22327801, and No. 22241302), the Innovation Program for Quantum Science and Technology (Grants No. 2021ZD0303102 and No. 2022YFF0606500), and the Chinese Academy of Sciences (Grant No. YSBR-055).

- 
- [1] E. J. Salumbides, G. D. Dickenson, T. I. Ivanov, and W. Ubachs, *Phys. Rev. Lett.* **107**, 043005 (2011).
  - [2] L. Wang and Z. C. Yan, *Phys. Chem. Chem. Phys.* **20**, 23948 (2018).
  - [3] M. Puchalski, J. Komasa, P. Czachorowski, and K. Pachucki, *Phys. Rev. Lett.* **122**, 103003 (2019).
  - [4] N. Hölsch, M. Beyer, E. J. Salumbides, K. S. E. Eikema, W. Ubachs, C. Jungen, and F. Merkt, *Phys. Rev. Lett.* **122**, 103002 (2019).
  - [5] J. Komasa, M. Puchalski, P. Czachorowski, G. Łach, and K. Pachucki, *Phys. Rev. A* **100**, 032519 (2019).
  - [6] L. G. Tao, A. W. Liu, K. Pachucki, J. Komasa, Y. R. Sun, J. Wang, and S. M. Hu, *Phys. Rev. Lett.* **120**, 153001 (2018).
  - [7] Q.-H. Liu, Y.-N. Lv, C.-L. Zou, C.-F. Cheng, and S.-M. Hu, *Phys. Rev. A* **106**, 062805 (2022).
  - [8] A. Fast and S. A. Meek, *Phys. Rev. Lett.* **125**, 023001 (2020).
  - [9] D. Mondelain, S. Kassı, and A. Campargue, *J. Quant. Spectrosc. Radiat. Transfer* **253**, 107020 (2020).
  - [10] A. Fast and S. A. Meek, *Mol. Phys.* **120**, e1999520 (2021).
  - [11] A. Castrillo, E. Fasci, and L. Gianfrani, *Phys. Rev. A* **103**, 022828 (2021).
  - [12] S. Kassı, C. Lauzin, J. Chaillot, and A. Campargue, *Phys. Chem. Chem. Phys.* **24**, 23164 (2022).
  - [13] S. Patra, M. Germann, J.-P. Karr, M. Haidar, L. Hilico, V. I. Korobov, F. M. J. Cozijn, K. S. E. Eikema, W. Ubachs, and J. C. J. Koelemeij, *Science* **369**, 1238 (2020).
  - [14] K.-F. Lai, V. Hermann, T. M. Trivikram, M. Diouf, M. Schlösser, W. Ubachs, and E. J. Salumbides, *Phys. Chem. Chem. Phys.* **22**, 8973 (2020).
  - [15] F. M. J. Cozijn, P. Dupré, E. J. Salumbides, K. S. E. Eikema, and W. Ubachs, *Phys. Rev. Lett.* **120**, 153002 (2018).
  - [16] F. M. J. Cozijn, M. L. Diouf, and W. Ubachs, *Phys. Rev. Lett.* **131**, 073001 (2023).
  - [17] Q.-H. Liu, Y. Tan, C.-F. Cheng, and S.-M. Hu, *Phys. Chem. Chem. Phys.* **25**, 27914 (2023).
  - [18] K. Bielska, A. A. Kyuberis, Z. D. Reed, G. Li, A. Cygan, R. Ciuryło, E. M. Adkins, L. Lodi, N. F. Zobov, V. Ebert, D. Lisak, J. T. Hodges, J. Tennyson, and O. L. Polyansky, *Phys. Rev. Lett.* **129**, 043002 (2022).
  - [19] S. L. Bragg, J. W. Brault, and W. H. Smith, *Astrophys. J.* **263**, 999 (1982).
  - [20] D. C. Robie and J. T. Hodges, *J. Chem. Phys.* **124**, 024307 (2006).
  - [21] A. Campargue, S. Kassı, K. Pachucki, and J. Komasa, *Phys. Chem. Chem. Phys.* **14**, 802 (2012).
  - [22] S.-M. Hu, H. Pan, C.-F. Cheng, Y. R. Sun, X.-F. Li, J. Wang, A. Campargue, and A.-W. Liu, *Astrophys. J.* **749**, 76 (2012).
  - [23] Y. Tan, J. Wang, C.-F. Cheng, X.-Q. Zhao, A.-W. Liu, and S.-M. Hu, *J. Mol. Spectrosc.* **300**, 60 (2014).
  - [24] E. Roueff, H. Abgrall, P. Czachorowski, K. Pachucki, M. Puchalski, and J. Komasa, *Astron. Astrophys.* **630**, A58 (2019).
  - [25] P. Wcisło, H. Tran, S. Kassı, A. Campargue, F. Thibault, and R. Ciuryło, *J. Chem. Phys.* **141**, 074301 (2014).
  - [26] M. Słowiński, H. Jóźwiak, M. Gancewski, K. Stankiewicz, N. Stolarczyk, Y. Tan, J. Wang, A.-W. Liu, S.-M. Hu, S. Kassı, A. Campargue, K. Patkowski, P. S. Żuchowski, R. Ciuryło, F. Thibault, and P. Wcisło, *J. Quant. Spectrosc. Radiat. Transfer* **277**, 107951 (2022).

- [27] F. Thibault, K. Patkowski, P. S. Żuchowski, H. Józwiak, R. Ciuryło, and P. Wcisło, *J. Quant. Spectrosc. Radiat. Transfer* **202**, 308 (2017).
- [28] M. Słowiński, F. Thibault, Y. Tan, J. Wang, A.-W. Liu, S.-M. Hu, S. Kassı, A. Campargue, M. Konefał, H. Józwiak, K. Patkowski, P. Żuchowski, R. Ciuryło, D. Lisak, and P. Wcisło, *Phys. Rev. A* **101**, 052705 (2020).
- [29] N. Stolarczyk, G. Kowzan, F. Thibault, H. Cybulski, M. Słowiński, Y. Tan, J. Wang, A.-W. Liu, S.-M. Hu, and P. Wcisło, *J. Chem. Phys.* **158**, 094303 (2023).
- [30] R. W. Drever, J. L. Hall, F. V. Kowalski, J. Hough, G. Ford, A. Munley, and H. Ward, *Appl. Phys. B* **31**, 97 (1983).
- [31] J. Wang, Y. R. Sun, L.-G. Tao, A.-W. Liu, and S.-M. Hu, *J. Chem. Phys.* **147**, 091103 (2017).
- [32] N. Ismail, C. C. Kores, D. Geskus, and M. Pollnau, *Opt. Express* **24**, 16366 (2016).
- [33] W. Demtröder, *Laser Spectroscopy I: Basic Principles* (Springer, New York, 2014).
- [34] A. Cygan, P. Wcisło, S. Wójtewicz, P. Masłowski, J. T. Hodges, R. Ciuryło, and D. Lisak, *Opt. Express* **23**, 14472 (2015).
- [35] A. Cygan, D. Lisak, P. Morzyński, M. Bober, M. Zawada, E. Pazderski, and R. Ciuryło, *Opt. Express* **21**, 29744 (2013).
- [36] K. Libbrecht and M. Libbrecht, *Amer. J. Phys.* **74**, 1055 (2006).
- [37] L. Rutkowski, A. C. Johansson, G. Zhao, T. Hausmaninger, A. Khodabakhsh, O. Axner, and A. Foltynowicz, *Opt. Express* **25**, 21711 (2017).
- [38] M. Nelkin and A. Ghatak, *Phys. Rev.* **135**, A4 (1964).
- [39] S. G. Rautian and I. I. Sobel'man, *Sov. Phys. Usp.* **9**, 701 (1967).
- [40] M. Konefał, M. Słowiński, M. Zaborowski, R. Ciuryło, D. Lisak, and P. Wcisło, *J. Quant. Spectrosc. Radiat. Transfer* **242**, 106784 (2020).
- [41] P. R. Berman, *J. Quant. Spectrosc. Radiat. Transfer* **12**, 1331 (1972).
- [42] A. Pine and R. Ciuryło, *J. Mol. Spectrosc.* **208**, 180 (2001).
- [43] P. L. Varghese and R. K. Hanson, *Appl. Opt.* **23**, 2376 (1984).
- [44] A. Cygan, D. Lisak, S. Wójtewicz, J. Domysławska, J. T. Hodges, R. S. Trawiński, and R. Ciuryło, *Phys. Rev. A* **85**, 022508 (2012).
- [45] P. Wcisło, I. E. Gordon, C.-F. Cheng, S.-M. Hu, and R. Ciuryło, *Phys. Rev. A* **93**, 022501 (2016).
- [46] P. Wcisło, I. Gordon, H. Tran, Y. Tan, S.-M. Hu, A. Campargue, S. Kassı, D. Romanini, C. Hill, R. Kochanov, and L. Rothman, *J. Quant. Spectrosc. Radiat. Transfer* **177**, 75 (2016).
- [47] H. Fleurbaey, A. Koroleva, S. Kassı, and A. Campargue, *Phys. Chem. Chem. Phys.* **25**, 14749 (2023).
- [48] A. Cygan, S. Wójtewicz, M. Zaborowski, P. Wcisło, R. Guo, R. Ciuryło, and D. Lisak, *Meas. Sci. Technol.* **27**, 045501 (2016).
- [49] D. Lisak, A. Cygan, S. Wójtewicz, P. Wcisło, M. Zaborowski, G. Kowzan, P. Masłowski, and R. Ciuryło, *J. Phys.: Conf. Ser.* **810**, 012007 (2017).
- [50] I. E. Gordon *et al.*, *J. Quant. Spectrosc. Radiat. Transfer* **277**, 107949 (2022).
- [51] M. L. Diouf, F. M. Cozijn, and W. Ubachs, *Mol. Phys.* **122**, e2304101 (2024).
- [52] A. L. Laraia, R. R. Gamache, J. Lamouroux, I. E. Gordon, and L. S. Rothman, *Icarus* **215**, 391 (2011).
- [53] R. R. Gamache, B. Vispoel, M. Rey, A. Nikitin, V. Tyuterev, O. Egorov, I. E. Gordon, and V. Boudon, *J. Quant. Spectrosc. Radiat. Transfer* **271**, 107713 (2021).
- [54] P. Werle, *Appl. Phys. B* **102**, 313 (2011).